Published in final edited form as:
Environ Sci Nano. 2014 April ; 1(2): 144–153. doi:10.1039/C3EN00062A.

Engineering safer-by-design, transparent, silica-coated ZnO nanorods with reduced DNA damage potential

Georgios A. Sotiriou[1], **Christa Watson**[1], **Kimberly M. Murdaugh**[1,2], **Thomas H. Darrah**[3], **Georgios Pyrgiotakis**[1], **Alison Elder**[4], **Joseph D. Brain**[1], and **Philip Demokritou**[1,*]

[1]Department of Environmental Health, Center for Nanotechnology and Nanotoxicology, School of Public Health, Harvard University, 665 Huntington Avenue, Boston, MA 02115, USA

[2]School of Engineering and Applied Sciences, Harvard University, 29 Oxford Street, Cambridge, MA 02138, USA

[3]School of Earth Sciences, 231 Mendenhall Laboratory, The Ohio State University, Columbus, OH 43210, USA

[4]University of Rochester, Department of Environmental Medicine, 601 Elmwood Avenue, Rochester, NY 14642, USA

Abstract

Zinc oxide (ZnO) nanoparticles absorb UV light efficiently while remaining transparent in the visible light spectrum rendering them attractive in cosmetics and polymer films. Their broad use, however, raises concerns regarding potential environmental health risks and it has been shown that ZnO nanoparticles can induce significant DNA damage and cytotoxicity. Even though research on ZnO nanoparticle synthesis has made great progress, efforts on developing safer ZnO nanoparticles that maintain their inherent optoelectronic properties while exhibiting minimal toxicity are limited. Here, a safer-by-design concept was pursued by hermetically encapsulating ZnO nanorods in a biologically inert, nanothin amorphous SiO_2 coating during their gas-phase synthesis. It is demonstrated that the SiO_2 nanothin layer hermetically encapsulates the core ZnO nanorods without altering their optoelectronic properties. Furthermore, the effect of SiO_2 on the toxicological profile of the core ZnO nanorods was assessed using the Nano-Cometchip assay by monitoring DNA damage at a cellular level using human lymphoblastoid cells (TK6). Results indicate significantly lower DNA damage (>3 times) for the SiO_2-coated ZnO nanorods compared to uncoated ones. Such an industry-relevant, scalable, safer-by-design formulation of nanostructured materials can liberate their employment in nano-enabled products and minimize risks to the environment and human health.

INTRODUCTION

Zinc oxide (ZnO) is a wide band-gap semiconductor with optical, piezoelectric, and dielectric properties that render it useful for a variety of applications, ranging from transistors,[1] light emitting diodes,[2] sensors,[3] photocatalysis,[4] and ultraviolet (UV)-filters,[5] to

*Correspondence to: pdemokri@hsph.harvard.edu.

name a few. When in nanoscale, ZnO exhibits several advantages. For example, the high electron mobility and diversity of ZnO nanostructures makes it a suitable material for dye-sensitized solar cells,[6] while its large surface-to-volume ratio may improve its bioavailability when employed in food-fortification applications.[7] Furthermore, ZnO nanoparticles exhibit luminescence and therefore may be used as novel labels *in vitro*.[8]

ZnO absorbs UV wavelengths ranging from 280 to 400 nm[5,9] making it an ideal component in cosmetic creams and sunscreens that aim to block both UVA (320–400 nm) and UVB (280–320 nm) radiation.[10] Traditional sunscreens use micron-sized ZnO particles that make them opaque with bright white color that is esthetically undesirable for consumers.[11–12] In contrast, ZnO nanoparticles are transparent to visible light yielding a less opaque sunscreen. As a result, ZnO nanoparticle-based sunscreens are favored and their production has increased dramatically in recent years.[11–12] Both wet- and gas-phase synthetic strategies have been employed to synthesize ZnO nanostructures, including chemical vapor deposition,[13] hydrolysis,[14] and flame synthesis[15–16] with various morphologies explored.

Because of the wide range of ZnO nanoparticle applications, exposure to humans is inevitable.[11] However, the potential adverse health effects of ZnO nanoparticle exposures have not been fully determined. *In vivo* and *in vitro* toxicological studies have shown that these particles are acutely toxic to alveolar epithelial cells and macrophages.[17–19] Additionally, ZnO nanoparticles have been reported to induce significant cytotoxicity and genotoxicity in human neuronal cells.[20] ZnO nanoparticles can also generate reactive oxygen species (ROS)[21] within human skin melanoma cells in acute exposures which led to DNA damage, cell viability reduction, and apoptosis.[22] Exposure via inhalation is of particular concern as reduced pulmonary function in humans was found 24hoursafter exposure to ZnO nanoparticles.[23] Furthermore, recent work in our group has shown that ZnO nanoparticles can cause high genotoxicity when compared to various industrially relevant metal nanomaterials such as silver, iron oxide, and cerium oxide.[24] The reported cytotoxicity and DNA damage associated with ZnO exposures is attributed to the released ions from its rapid dissolution within aqueous solutions, but also from direct particle interactions with cells through the induction of oxidative stress.[19,25]

Therefore, minimizing the ZnO nanoparticle dissolution and direct contact with the cells can greatly inhibit toxicity.[26] Such a safer-by-design formulation concept for the gas-phase synthesis of metal oxide nanoparticles by a modified flame spray pyrolysis (FSP) reactor[27] has been recently developed by the authors and involves the encapsulation of the core nanoparticles with a nanothin amorphous silica (SiO_2) layer.[17] The SiO_2 nanothin layer is formed by the swirl injection of Si-precursor vapor within the reactor after the core nanoparticle growth has ceased, allowing for a precise control over the coating thickness.[27] Such a nanothin amorphous SiO_2 coating preserves the functional inherent properties of the core material.[27]

Amorphous fumed nanostructured SiO_2 is considered biologically inert[28] and commonly used in cosmetic and personal care products and as a negative control in nanoparticle toxicity screening assays.[29] At high doses (> 100 μg/mL), amorphous SiO_2 may exhibit some *in vitro* toxicity[30–31] which is associated with the presence of strained three-membered

rings and the subsequent free radical formation.[31] However,*in vivo* studies using a rat model have verified that such a biological response is transient[32] and at lower, physiologically relevant doses, a flame-made SiO_2 coating has minimal lung injury and inflammation.[33] Furthermore, it was also demonstrated that the SiO_2 coating improves nanoparticle biocompatibility *in vitro* on a variety of nanomaterials including Ag,[34] Y_2O_3,[35] and ZnO nanoparticles and mammalian cell lines.[17]

Here, we explore the gas-phase synthesis of free-standing uncoated and hermetically SiO_2-coated (23 wt% SiO_2) ZnO nanorods by the flame spray pyrolysis (FSP) based Harvard Versatile Engineered Nanomaterial Generation System (VENGES).[36] Themorphology and physicochemical characteristics of the as-prepared nanoparticles are investigated using X-ray diffraction, N_2 adsorption, thermogravimetric analysis and electron microscopy, while the hermetic nature of the SiO_2 coating is evaluated by X-ray photoelectron spectroscopy, the inhibition of the photocatalytic methylene blue degradation and by measuring the ζ-potential across a broad pH range. The effect of the SiO_2 coating on the optoelectronic properties (UV-vis transmission and band-gap) of the core ZnO nanorods is also investigated in detail providing valuable information on the functionality of the SiO_2-coated nanoparticles and their application as efficient UV blockers. Most importantly, the effect of the SiO_2 shell on the genotoxicity of both uncoated and SiO_2-coated ZnO nanorods is evaluated using the Nano-Cometchip[24,37] bioassay while the cellular viability is also monitored by the reduction of a tetrazolium dye.

MATERIALS AND METHODS

Synthesis and Characterization

Uncoated and SiO_2-coated ZnO particles were synthesized by Flame Spray Pyrolysis (FSP) of zinc naphthenate (Sigma-Aldrich) dissolved in ethanol (Sigma-Aldrich) at a precursor molarity of 0.5 M. The precursor solution was fed through a stainless steel capillary at 5 mL/min, dispersed by 5 L/min O_2 (Air Gas, purity >99%, pressure drop at nozzle tip: p_{drop} = 2 bar) and combusted. A premixed methane-oxygen (1.5 L/min, 3.2 L/min) supporting flame was used to ignite the spray. O_2 (Air Gas, purity >99%) sheath gas was used at 40 L/min. Core particles were coated in-flight by the swirl-injection of HMDSO vapor (Sigma Aldrich) through a torus ring with 16 jets at an injection height of 200 mm above the FSP burner. The torus ring jet injection angles were 20° in downstream direction, in order to avoid stagnation flow, and 10° away from the centerline, in order to induce mixing. The reactor was enclosed by two quartz tubes: below and above the torus ring. A total gas flow of 16 L/min, consisting of N_2 carrying HMDSO vapor and pure N_2, was injected through the torus ring jets. HMDSO vapor was obtained by bubbling N_2 gas through liquid HMDSO (500 mL), maintained at a controlled temperature using a water bath. A theoretical coating thickness of ~5 nm was targeted assuming saturation conditions. After synthesis, particles were collected on a water-cooled glass fiber filter (What man) located 800 mm above the reactor with the aid of a vacuum pump.

For the electron microscopy analysis, uncoated and SiO_2-coated ZnO nanoparticles were dispersed in ethanol at a concentration of 1 mg/mL in 50 mL polyethylene conical tubes and sonicated for 10 minutes with sonication power of 1.75 Watt (Branson Sonifier S-450A).

The samples were deposited onto lacey carbon TEM grids. All grids were imaged with a JEOL 2100.

X-ray Diffraction (XRD) patterns for uncoated ZnO and SiO_2-coated ZnO nanoparticles were obtained using a Bruker D8 diffractometer (Cu K_α, λ = 0.154 nm, 40 kV, 40 mA, stepsize = 0.02°). 100 mg of each sample was placed onto the diffractometer stage and analyzed from a range of 2θ = 20–70°. Major diffraction peaks were identified using the Inorganic Crystal Structure Database (ICSD) for wurtzite (ZnO) crystal. The crystal size was determined by applying the Rietveld analysis of the major diffraction peaks. The specific surface area was obtained according to Brunauer-Emmet-Teller (BET) by five-point N_2 adsorption at 77 K (Micrometrics Tristar 3000). Prior to that, samples were degassed in N_2 for at least 1 h at 150 °C.

For the X-ray photoelectron spectroscopy analysis, 5 mg of powder was deposited on a metal sample holder coated with electrical tape and placed on the XPS sample stage (ESCA SSX-100). Soft X-rays from an Al anode are used to bombard the sample and eject electrons from the surface (monochromatic Al Kα, 10 kV, 10 mA). The KE of the ejected electrons was determined by a detector hemispherical electron energy spectrometer (spot size: 600 μm). The samples were scanned (BE range: 0 – 1100 eV, pass energy: 100 eV, step size: 0.65 eV), and the resulting spectra was analyzed with software (CASA XPS) and calibrated with the C 1s hydrocarbon contamination peak (BE: 284.6 eV). XPS was also used to determine the ratio of the elemental concentration of the core particle to the total elemental concentration of the entire nanoparticle.[17] This ratio, X_{el}, is defined as follows (Eq. 1):

$$X_{el} = \frac{ZnO_{core}}{ZnO_{core} + Si} \quad \text{(Eq. 1)}$$

where Me_{core} and Si are the elemental concentrations of the core ZnO and Si, respectively.

For the ζ-potential measurements, uncoated ZnO and SiO_2-coated ZnO nanoparticles were dispersed in deionized water (5 mg/mL) and placed in a 3 in. cup horn and sonicated with a Branson Sonifier S-450A (Branson Ultrasonics; Danbury, CT) for 10 minutes as described above. The liquid conical tube was submersed in the DI H_2O so that the level of the tube contents aligned with the surrounding DI H_2O. Hydrochloric acid (HCl) and potassium hydroxide (KOH) (both 0.1 M) were added to the suspensions to vary the pH between 2 and 13 pH, as measured by a SympHony pH meter (VWR International; Radnor, PA). 1 mL aliquots of each sample were placed in a cuvette analyzed for their zeta potential with a Malvern Zetasizer Nano ZS (Malvern Instruments; Worcestershire, UK). Zeta potential measurements were repeated in triplicate.

Methylene blue (Aldrich, MB) was employed as a model dye to evaluate the photocatalytic activity of the as-prepared nanoparticles. For each condition, 18 mg of particles was dispersed in 20 mL of 10 ppm MB aqueous solution. The pH during the photocatalytic activity experiments was ~6.8 ± 0.5. The beaker containing the particles and solution was placed on a magnetic stirrer plate and a stirrer bar placed in the solution ensured full suspension of the particles throughout the experiment. Prior to this, the suspensions were sonicated in a water bath (Branson Sonifier S-450A) for 30 s. Before UV-irradiation, the

suspensions were left for 30 min in the dark to equilibrate any adsorption-desorption effects. The photocatalytic reaction was conducted at room temperature under UV light from a single 9 W UV tube at 254 nm (Philips) positioned horizontally above (2 cm) the liquid surface. Each experiment was conducted for 45 min with 1 mL sample aliquots extracted after 10, 20, 30 and 45 min and were immediately centrifuged at 10,000 g. The decomposition of MB was monitored by measuring the absorbance of the supernatant using a UV–vis spectrophotometer (Agilent Cary 50, at 661 nm) in liquid cuvette configuration with de-ionized water as reference.

For the UV-vis transmission measurements, nanoparticles were dispersed in DI H_2O (0.5 mg/mL) in 50 mL polyethylene conical tubes. The samples were placed in a 3 in. cup horn and sonicated for 10 minutes as previously described. The samples were dispersed with a cup sonicator immediately prior to spectral analysis. 2 mL of the each dispersion was placed in a quartz cuvette and placed in the UV–vis spectrophotometer (Agilent Cary 50). UV-vis transmission measurements were performed over a spectrum of 190 to 900 nm with a reference background for DI H_2O. Dynamic light scattering (DLS) of such suspensions was performed using a Zetasizer Nano-ZS (Malvern Instruments, Worcestershire, UK). Diffuse reflectance measurements of the dry powders were performed on a Varian Cary 500 spectrophotometer. Samples were placed in a dry powder sample holder (Praying Mantis).

For the dissolution investigation of both uncoated and SiO_2-coated ZnO nanorods, nanoparticles were dispersed in culture media (RPMI-1640 with L-glutamine supplemented with 10% horse serum and 100 units/mL penicillin and streptomyocin, pH = 7.4, total concentration of inorganic salts [ionic strength] = 139.1 mM) by sonication[38] at a concentration of 100 mg/L of ZnO. Samples (1 mL) were taken over time for 24 h, and immediately centrifuged to 10,000 g for 1 h. Then the supernatant was taken and stored for further analysis. The experiment was conducted in triplicate.

All sample preparation for ICP-MS analysis was conducted in a Class 100 trace metal-free clean laboratory. For the dissolution fractions, approximately 1.0 mL of each sample was transferred to the corresponding pre-labeled analytical vials and verified gravimetrically to ±0.002 mg using Perkin Elmer AD6 microbalance. Next, the samples were digested in ultra-pure nitric acid (15.9 mol/L) and concentrated hydrochloric acid (12.4 mol/L) (Thermo Fisher Scientific, Waltham, MA, USA) and baked at 80°C for 6 hours. After sample digestion was verified visually, the samples were decanted by baking at 60°C until dry (~12 hours). All samples (and standards) were diluted and prepared for analysis using water purified to 18.2 MΩ cm resistance using a Milli-Q water purification system (Millipore, Bedford, MA, USA), acidified using trace metal-free concentrated (15.9 mol/L) ultra-pure nitric acid (Thermo Fisher Scientific, Waltham, MA, USA), and spiked with internal standards consisting of known quantities of indium (In) and bismuth (Bi), to monitor instrumental behavior and sample response similar to methods reported previously.[39]

Silicon and zinc were measured using a Perkin Elmer DRC II ICP-MS at Ohio State University consistent with previous methods.[39–40] External calibration standards used to determine Si, Zn, and other metal concentrations in analytical samples were spiked with known quantities of each analyte (e.g., Si, Zn, etc.) in a linear range (e.g. from 0.05 to 20.0

μg/g). All standards were prepared from 1000 mg/L single element standards obtained from SCP Science, USA. Isobaric corrections were performed on-line using ICP-MS software. Five duplicate analyses (n=5) were performed for each analyte for all sample solutions. Average reproducibility based on replicate analysis of known-unknown external calibration standards was 3.06%. The LOD and LOQ for Si were 0.108 ng/g and 0.213 ng/g, respectively. The LOD and LOQ for Zn were 0.016 ng/g and 0.034 ng/g, respectively. Method detection limits were calculated according to the two-step approach using the t99SLLMV method at 99% CI (t=3.71). The calculated MDL for Si and Zn were 0.890 ng/g and 0.080 ng/g, respectively. The external precision for all analytes was less than 5% for all reported analysis.

DNA damage and cytotoxicity evaluation

For the cell culture and treatment, human lymphoblastoid cells, TK-6, were a kind gift of Bevin Engelward from MIT. Human lymphoblastoid cell line, TK6, was chosen for these experiments as they are routinely used in using the comet assay method and genotoxicity assessments.[41] Additionally, TK6 cells are p53 proficient and genetically stable, which are essential attributes in the detection of genotoxic agents.[42] Moreover, the decision to use this particular cell line was not based on physiological relevance but in the effort to detect minute differences in the genotoxic response to these similar materials. Cells were maintained in RPMI-1640 with L-glutamine supplemented with 10% horse serum and 100 units/mL penicillin and streptomyocin (pH = 7.4, total concentration of inorganic salts [ionic strength] = 139.1 mM) at 37 °C in an atmosphere of 5% CO_2/95% air. Cells were seeded for treatment in a 96-well plate at a density of 2×10^6 cells/well in 100 μL. Nanoparticle suspensions were prepared and sonicated as mentioned below in Cohen *et al.*[38] in 3 mg/mL concentrated stocks in sterile distilled water. The stocks were then diluted in RPMI media containing 10% horse serum to the appropriate concentration (5, 10, 20 μg/mL). Each suspension was vortexed prior to adding to the cells at a volume of 100 μL for 4 hours.

DNA damage evaluation were performed as described in Watson *et al.*,[24] in which the customization of the Cometchip platform[37,43] was successfully performed for investigating the genotoxicity of various metals and metal oxides nanoparticles. For the Nano-Cometchip preparation and cell loading, negative silicon molds for polydimethylsiloxane (PDMS) casting of patterned microposts were made. The resulting PDMS mold was allowed to set in molten 1% normal melting point agarose applied to gel bond film for 20 minutes. After agarose polymerization, the PDMS stamp was removed revealing a thick gel consisting of arrayed microwells. The gel was then clamped between a bottomless 96 well plate and a glass plate. Pre-exposed cells were then added to the microwell array and allowed to load for 30 minutes. After gravitational settling of cells had occurred, excess cells were aspirated and the gel was rinsed three times with warm phosphate buffered saline. Molten low melting agarose was used to cover microwell array/cells and allowed to set for 5 minutes at room temperature and 5 minutes at 4 °C. The gel was then submerged into lysis solution containing (2.5 M NaCl, 100 mM Na_2 EDTA, 10 mM Tris, pH 9.5 with 0.5% Triton X-100) overnight at 4 °C. After lysis, gels were washed two times in PBS to remove surfactant. Gels were then adhered to electrophoresis inner tank well with double sided tape (gel side up). Electrophoresis was then performed using alkaline buffer (90 mM Tris, 90 mM Boric Acid,

2 mM Na_2 EDTA, pH 8.5) at 4 °C for 30 min at 25 V and 300 mA. Imaging and data collection was performed using an automated fluorescent microscope (Axiovert Zeiss) and proprietary MatLab software was used to analyze data sets. The median of % DNA in tail was utilized to obtain the amount of DNA damage within the cell population at each dosage. The reported values are the average of at least six experiments along with the standard error. P-values less than 0.05 were considered to be significant.

For the cellular viability evaluation, the MTT assay (Roche) was used to assess the mitochondrial dehydrogenase activity of intact and injured TK6 cells exposed to nanoparticles. TK6 cells, a suspension lymphoblastoid cell line, were seeded into 96 well plates at a density of 1×10^4 cells/well in RPMI media in 100 μL containing 10% horse serum. Nanoparticle suspensions were added at 100 μL at twice the concentration needed to obtain 5, 10, 20 μg/mL for 4hrs at 37 °C in 5% CO_2. After exposure, cells were spun down at 250g and spent media was aspirated. Fresh media was then added and MTT reagent (3-[4,5-dimethylthiazol-2-yl]-2,5-diphenyl tetrazolium bromide) (10 μL) was added to each well for a period of 4 hours at 37 °C. Solubilization reagent (150 μL) was added to dissolve the formazan crystals produced from the reduction of the tetrazolium salt or MTT reagent in viable cells. Absorbance was measured at 550 nm using a Molecular Devices microplate reader. A cellular experiments were performed to ensure reagent integrity and to rule out NP interference. The data obtained revealed no interaction between test nanoparticles and MTT reagents during the 4 hours exposure time point. Percent cell viability (relative viability compared to untreated cells) was calculated as mean value ± standard error of the mean (SEM) as a result of three independent experiments performed in triplicate.

RESULTS AND DISCUSSION

Nanoparticle morphology

The morphology of the as-prepared nanoparticles was evaluated qualitatively by electron microscopy. Figure 1 shows transmission electron microscopy (TEM) images of the uncoated (a, b) and SiO_2-coated (c, d) ZnO nanoparticles. From the TEM images it appears that the ZnO nanoparticles are not spherical but rather rod-like. Flame-made nanoparticles typically exhibit a log-normal particle size distribution ($\sigma_g = 1.45$),[44] while the ZnO nanorod aspect ratio ranges from 2 to 8 with an average ~3 and this is in agreement with similar studies reported in the literature.[45] ZnO nanorods have been made before by flame spray pyrolysis in the presence of dopants (indium and tin up to 10 at%).[46] Such doping, however, influences their optoelectronic properties,[46] thus making these nanorods unsuitable for a number of applications where purity is important. In contrast here, pure ZnO nanorods are made while their formation is attributed to particle annealing and rearrangement within the flame,[46] and the long residence time at high temperatures typical for enclosed FSP reactors.[27] Even though the nanorod morphology is not required specifically for their employment as UV-filters, such nanostructures may find applications in other fields, such as nanoelectronics.[45] Furthermore, for the SiO_2-coated sample (c, d) there is a ~4.5 nm thick homogeneous amorphous layer encapsulating the core crystalline ZnO nanoparticles.[17] The SiO_2 coating thickness distribution on the ZnO nanorods is shown in the inset of Figure 1d, along with the average value ± the standard deviation, as well as the total number N of

coatings counted. Furthermore, there are few, if any, free SiO_2 nanoparticles further verifying the coating efficiency of the reactor.[47]

X-ray diffraction (XRD) was utilized to assess the crystal structure and size of the as-prepared pristine nanoparticles. Figure 2 shows the diffraction patterns of both uncoated (black) and SiO_2-coated (red) ZnO nanorods. Both patterns have the characteristic peaks corresponding to the wurtzite crystal structure.[16] Furthermore, the diffraction peaks of both coated and uncoated samples coincide, verifying that the underlying ZnO core particles have identical crystallinity. The average crystal size for both samples is ~30 nm. This further indicates that the SiO_2 coating formation does not influence the ZnO core nanoparticle growth that had already stopped before the injection of the SiO_2 precursor vapor within the coating reactor.[17,27]

It is also worth mentioning that there are no diffraction peaks corresponding to Zn-silicates. Under specific conditions during the nanoparticle synthesis, Zn-silicate formation can occur, especially when high specific combustion enthalpy solvents are used that can increase the reactor temperature profile.[17,48] However, a low specific combustion enthalpy solvent was deliberately chosen (please see Materials and Methods section) since the Zn-silicate formation was undesired. There are also no signs of any highly toxic[32] crystalline SiO_2 diffraction peaks, further verifying that the SiO_2 is amorphous.[27] This is expected for flame-made SiO_2 nanoparticles.[49] Furthermore, the specific surface area (SSA) values of the uncoated, and SiO_2-coated ZnO nanorods are similar (Figure 2, inset) indicating that there are few or no separate SiO_2 nanoparticles that would lead to larger (>100 m^2/g) SSA values.[47,50] This is also in qualitative agreement with the absence of such free SiO_2 particles from the TEM analysis (Figure 1c).

SiO_2 coating encapsulation efficiency

The hermetic nature of the SiO_2 coating was evaluated using multiple techniques. First, X-ray photoelectron spectroscopy (XPS) was employed, a surface sensitive technique that allows for the coating efficiency quantification on nanostructured materials.[17] The XPS spectra of both uncoated (black) and SiO_2-coated (red) ZnO nanorods are shown in Figure 3a. The characteristic peaks corresponding to the Zn (diamonds) and Si (circles) metal electron transitions are also shown. When both spectra are compared, the Zn peaks are significantly reduced for the SiO_2-coated sample, even though the SiO_2 mass fraction is 23 wt%. It should be noted that the Zn peaks do not completely disappear. This could be attributed to two factors; (i) the inelastic mean free path of lower energy Zn electrons that can penetrate through the nanothin SiO_2 layer,[51](ii) a small fraction of the core particles escape the coating process and remain partially uncoated.[52] This is also evidenced by the coating efficiency which was found to be 95 % here (Figure 3a, inset), as calculated by the XPS spectra using the elemental concentration of Zn and Si atoms (please see Materials and Methods section, Eq. 1).[17]

Due to the aforementioned limitation of XPS, the hermetic nature of the SiO_2 coating was further evaluated by monitoring the ζ-potential of the uncoated and SiO_2-coated nanoparticles over a range of pH values. Figure 3b shows the ζ-potential of uncoated (triangles) and SiO_2-coated (circles) nanoparticles for pH = 2.5–8. Pure ZnO nanorods have

an isoelectric point around pH = 8,[53] while the SiO_2-coated nanorods retain a negative ζ-potential for the same pH range, in agreement with the ζ-potential of pure SiO_2.[47] This indicates that there is no significant ZnO surface exposed, and most importantly, such SiO_2-coated ZnO nanorods behave like SiO_2 nanoparticles in aqueous solutions and in biological media.[17,54]

The photocatalytic activity of the ZnO nanorods was also examined. Upon UV irradiation on ZnO nanorods, the electron-hole pairs on the particle surface participate in redox reactions with organic species, such as methylene blue (MB), that lead to their degradation.[55] Therefore, monitoring the MB degradation over time in aqueous solutions upon UV irradiation gives a good estimate on the ZnO surface availability and reactivity. Figure 3c shows the MB degradation as a function of time using the as-prepared uncoated (black line) and SiO_2-coated ZnO nanorods (red line). Photocatalytic TiO_2 nanoparticles (green line, P25) were used as a positive control. It can be seen that the uncoated ZnO nanorods are highly photocatalytic[4] and they slightly outperform the "gold standard" P25 TiO_2 nanoparticles completely decomposing MB after 30 min. In contrast, the SiO_2-coated ZnO nanorods show no photocatalytic activity because of the small uncoated ZnO surface fraction (<5%). This verifies that the SiO_2 coating hermetically encapsulates the core ZnO nanorods.[17]

It is noteworthy that gas-phase synthesis results in high purity products[56] and that there is no organic contamination on the SiO_2 surface. This is further verified here by thermogravimetric analysis of the SiO_2-coated ZnO nanorods. Figure 3d shows the sample mass percentage as a function of time. The measured mass loss is < 1% for up to 700 °C, typical for impurity-free flame-made nanoparticles.[57] Furthermore, given that the surface chemistry of SiO_2 is very well-understood,[58–59] the SiO_2 shell on the ZnO core can facilitate further surface (bio) functionalization which can increase the nanorod functionality and versatility for a variety of bio-applications. It is noteworthy that typical wet-made SiO_2 coatings on nanoparticles are porous,[60] therefore allowing ion release. However, dry-coated[27,34] nanoparticles typically yield a dense non-porous nanothin coating completely isolating the core material from its environment. Figure 4 shows the dissolved Zn fraction (%) as a function of time for both uncoated and SiO_2-coated ZnO nanorods (ZnO concentration of 100 mg/L) in cell culture medium (pH = 7.4, total concentration of inorganic salts [ionic strength] = 139.1 mM). The uncoated ZnO nanorods continuously dissolve up to 24 h without reaching equilibrium. In contrast, the SiO_2-coated ZnO nanorods also exhibit an initial ZnO dissolution, however it appears that after 6 h the system has reached equilibrium. In the case of the SiO_2-coated ZnO nanorods the core dissolution most probably originates from the small uncoated ZnO surface fraction (<5%). This indicates that even though the surface coating has a high efficiency (>95%), as soon as there is some core surface exposed a large fraction of the core ZnO is dissolved, as expected, but it is still lower than the case on uncoated ZnO nanorods. Furthermore, the SiO_2 coating is rather stable in the cell medium as over 24 h as it only dissolves <8% (data not shown). These results are in agreement with dissolution data of both SiO_2 and ZnO in culture media published in the literature.[61]

Effect of SiO_2 coating on optoelectronic properties

A fundamental prerequisite for the successful utilization of these safer-by-design ZnO nanorods is the preservation of their desired optoelectronic properties. Figure 5a shows the transmission (%) spectra of aqueous suspensions of uncoated (black line) and SiO_2-coated (red line) ZnO nanorods (0.5 mg/mL of ZnO). Both samples exhibit relatively high transmittance in the visible range 400 – 700 nm with the SiO_2-coated ZnO nanorods outperforming (>80%) the uncoated ones. This increase in transmittance is attributed to the lower hydrodynamic size and better dispersibility in aqueous solution of SiO_2-coated ZnO nanorods in comparison to uncoated ones: the coated ones have slightly lower agglomerate size in pure DI water than the uncoated ones (165 vs 220 nm), while in cell media both particles have similar agglomeration state (210 vs 220 nm).[17] The ζ-potential of ZnO nanorods at pH = 6.5 – 8.5 is close to zero that allows the formation of larger agglomerates (Figure 3b, black line). In contrast, the pH of SiO_2-coated ZnO nanorods at this pH range is highly negative (Figure 3b, red line), resulting in a highly-stable suspension with low hydrodynamic diameter. The lower hydrodynamic diameter of the SiO_2-coated ZnO nanorods results in less light scattering and high transmittance. However, both samples show a strong decrease in transmittance for wavelengths below 400 nm indicating the strong UV absorption of ZnO nanorods.[10]

The optoelectronic properties of both uncoated and SiO_2-coated ZnO nanorods are further evaluated by measuring their band-gap, E_g. Figure 5b shows the diffuse-reflectance spectra (Kubelka-Munk function F(R)) of both uncoated (black line) and SiO_2-coated ZnO nanorods (red line). The curves for both samples overlap and therefore these two samples have identical band-gaps (~3.3 eV), in agreement with the theoretical value.[10] This is in line with the identical crystallinity of these samples (Figure 2) and further verifies that the presence of the SiO_2 coating does not influence the optoelectronic properties of the core ZnO nanorods, rendering them highly transparent (in the visible range) UV-filters that may be employed in sunscreens and polymer nanocomposites.

Effect of SiO_2 coating on DNA damage and cytotoxicity

The DNA damage in human lymphoblastoid cells (TK-6) exposed to both uncoated and SiO_2-coated ZnO nanorods was evaluated using the Nano-Cometchip cellular assay.[24,37,43]Figure 6a shows the % DNA tail (damage) of cells incubated for 4 hours with uncoated and SiO_2-coated ZnO nanorods at ZnO concentrations of 5 (blue bars), 10 (green bars) and 20 μg/mL (red bars). H_2O_2 (100 μM) was used as a positive control, pure SiO_2 nanoparticles (SSA = 185 m^2/g) and cell culture medium (white bar, no particles) as negative controls. For all concentrations, pure SiO_2 nanoparticles do not exhibit strong DNA damage (≤20%), further verifying their relatively inert nature. The SiO_2 DNA damage is slightly higher than that of pure medium, which could be attributed to the high SiO_2 surface area concentration in solution (1–4 m^2/L). The ZnO nanorods are not fully dissolved for the incubation period here, thus it is expected that both the uncoated and SiO_2-coated nanorods are internalized by the cells. Such SiO_2-coated nanoparticles uptake can be qualitatively detected by TEM analysis. As indicated in a study recently published by the authors, SiO_2-coated ZnO nanorods were indeed internalized by cells.[62]

Pure uncoated ZnO nanorods induce a strong dose-dependent DNA damage and at the highest dose are comparable to the positive control (H_2O_2), which is in agreement with published studies.[20,22,24] In contrast, SiO_2-coated ZnO nanorods exhibit significantly less DNA damage in comparison to the uncoated ones. For concentrations up to 10 μg/mL, the SiO_2-coated ZnO nanorods do not exhibit any DNA damage at all, similar to pure medium. At the highest concentration of 20 μg/mL, the DNA damage of the SiO_2-coated ZnO nanorods is slightly higher than that of the control and pure SiO_2. However, the DNA damage induced by the uncoated ZnO nanorods at that concentration (20 μg/mL) is much higher (~3 times) than that of the SiO_2-coated ZnO nanorods. Therefore, the nanothin amorphous SiO_2 coating on the ZnO surface clearly exhibits a protective effect and inhibits the strong DNA damage induced by the core ZnO nanorods.

Figure 6b illustrates the cell viability for pure SiO_2, uncoated, and SiO_2-coated ZnO nanorods for 5 (blue bars), 10 (green bars) and 20 μg/mL (red bars) as determined by the MTT assay after 4 hours of incubation. None of the particles exhibited strong cytotoxicity. Reductions in viability were observed in TK-6 cells exposed to both uncoated and SiO_2-coated ZnO nanorods at the highest dose (20μg/mL). This decrease, however, was less than the half maximal inhibitory concentration or IC_{50}, as only 25% reductions were found. This is expected here for all samples because of their limited exposure period (4 hours). For longer exposures (24 h), a clear protective effect was detected for the SiO_2-coated ZnO nanorods.[17] This result highlights that even though there is no significant cytotoxicity observed, DNA damage (Figure 6a) may be present at low, sublethal cellular doses. It is worth pointing out that in genotoxicity studies, it is important to evaluate cytotoxicity in correlation with DNA damage, as they are both interrelated. When assessing cytotoxicity using metabolic function as an endpoint, cellular viability of 50% and above are acceptable levels of cell death, which do not interfere with genotoxicity evaluations.[63] Thus, the observed results using the MTT analysis suggests that moderate amounts of cytotoxicity were induced by exposure to the utilized concentrations for both coated and uncoated nanoparticles and no interference with genotoxicity assessment occurs here.

CONCLUSIONS

The above DNA damage results indicate that a hermetic SiO_2 shell on ZnO nanorods minimizes their nanobio interactions significantly reducing their genotoxicity, in agreement with the biologically inert nature of amorphous SiO_2. This SiO_2 shell protective effect might be attributed to the inhibition of the core ZnO dissolution, as well as the direct contact minimization of the cells with the ZnO surface. Amorphous SiO_2 is quite stable in water and biological media[61] not allowing, therefore, the core ZnO nanorod dissolution. It should be noted that it is possible to reduce the ZnO nanoparticle dissolution and mitigate the toxicity of similar flame-made ZnO nanoparticles by iron-doping (1–10 at% Fe) during their synthesis.[26,64] However, such doping changes the electronic configuration, band-gap and color of the ZnO nanoparticles, reducing their transparency in the visible spectrum. This effect makes the iron-doped ZnO nanoparticles unsuitable for their employment as transparent UV-filters in cosmetic products or polymer films. In contrast, by applying a nanothin amorphous SiO_2 coating on ZnO nanoparticles, the DNA damage is minimized while all desired optoelectronic properties are maintained.

In conclusion, we present here the rational design and engineering of safer functional ZnO nanorods that fulfill all performance requirements for their broad employment as UV-filters in cosmetics and personal care products as well as polymers. By hermetically encapsulating these ZnO nanorods during their synthesis with a nanothin, amorphous SiO_2 shell, the core ZnO nanobio interactions are minimized. Furthermore, the SiO_2 coating facilitates the nanoparticle dispersion in solution, improving their transparency in the visible spectrum. The presence of SiO_2 does not influence the optoelectronic properties of the core ZnO nanorods so they retain their desired high transparency in the visible spectrum and UV absorption rendering them suitable for UV blocking applications. Most importantly, the SiO_2-coating on the ZnO nanorods significantly reduces the strong DNA damage that is otherwise observed for the pure uncoated ZnO nanorods. Such safer-by-design core-shell ZnO nanoparticles can be broadly employed in commodities without any performance loss and with reduced hazard to the environment and human health.

Acknowledgments

The authors thank Samuel Gass for the help with the nanoparticle synthesis, Profs. Sotiris E. Pratsinis (ETH Zurich) and Evelyn Hu (Harvard University) for discussions, B. Engelward (MIT) for providing the TK-6 cells and the Cometchip assay. This research was supported with an NSF (1235806) and NIEHS grant (ES 0000002). Georgios A. Sotiriou gratefully acknowledges the Swiss National Science foundation for the *Advanced Researcher* fellowship (grant no. 145392). Christa Watson is funded by the NIH – NHLBI Ruth L. Kirschstein T32 training grant (NIH HL007118). Kimberly M. Murdaugh was supported with an NSF Graduate Research Fellowship grant (DGE-1144152).

REFERENCES

1. Sun B, Sirringhaus H. Nano Lett. 2005; 5:2408–2413. [PubMed: 16351187]
2. Konenkamp R, Word RC, Godinez M. Nano Lett. 2005; 5:2005–2008. [PubMed: 16218727]
3. Wang JX, Sun XW, Yang Y, Huang H, Lee YC, Tan OK, Vayssieres L. Nanotechnology. 2006; 17:4995–4998.
4. Height MJ, Pratsinis SE, Mekasuwandumrong O, Praserthdam P. Appl. Catal. B-Environ. 2006; 63:305–312.
5. Becheri A, Durr M, Lo Nostro P, Baglioni P. J. Nanopart. Res. 2008; 10:679–689.
6. Anta JA, Guillen E, Tena-Zaera R. J. Phys. Chem. C. 2012; 116:11413–11425.
7. Hilty FM, Arnold M, Hilbe M, Teleki A, Knijnenburg JTN, Ehrensperger F, Hurrell RF, Pratsinis SE, Langhans W, Zimmermann MB. Nat. Nanotechnol. 2010; 5:374–380. [PubMed: 20418865]
8. Tang X, Choo ESG, Li L, Ding J, Xue J. Langmuir. 2009; 25:5271–5275. [PubMed: 19397360]
9. King DM, Liang X, Carney CS, Hakim LF, Li P, Weimer AW. Adv. Funct. Mater. 2008; 18:607–615.
10. Janotti A, Van de Walle CG. Rep. Prog. Phys. 2009; 72
11. Nohynek GJ, Dufour EK, Roberts MS. Skin Pharmacol. Physiol. 2008; 21:136–149. [PubMed: 18523411]
12. Nohynek GJ, Lademann J, Ribaud C, Roberts MS. Crit. Rev. Toxicol. 2007; 37:251–277. [PubMed: 17453934]
13. Galoppini E, Rochford J, Chen H, Saraf G, Lu Y, Hagfeldt A, Boschloo G. J. Phys. Chem. B. 2006; 110:16159–16161. [PubMed: 16913732]
14. Zhang Q, Chou TR, Russo B, Jenekhe SA, Cao G. Angew. Chem.-Int. Edit. 2008; 47:2402–2406.
15. Madler L, Stark WJ, Pratsinis SE. J. Appl. Phys. 2002; 92:6537–6540.
16. Tani T, Madler L, Pratsinis SE. J. Nanopart. Res. 2002; 4:337–343.
17. Gass S, Cohen JM, Pyrgiotakis G, Sotiriou GA, Pratsinis SE, Demokritou P. ACS Sustainable Chem. Eng. 2013; 1:843–857. [PubMed: 23961338]

18. Warheit DB, Sayes CM, Reed KL. Environ. Sci. Technol. 2009; 43:7939–7945. [PubMed: 19921917]
19. Xia T, Kovochich M, Liong M, Maedler L, Gilbert B, Shi H, Yeh JI, Zink JI, Nel AE. ACS Nano. 2008; 2:2121–2134. [PubMed: 19206459]
20. Valdiglesias V, Costa C, Kilic G, Costa S, Pasaro E, Laffon B, Teixeira JP. Environ. Int. 2013; 55:92–100. [PubMed: 23535050]
21. Shu-Feng H, Bello D, Schmidt DF, Pal AK, Stella A, Isaacs JA, Rogers EJ. Small. 2013; 9:1853–1865. [PubMed: 23423873]
22. Alarifi S, Ali D, Alkahtani S, Verma A, Ahamed M, Ahmed M, Alhadlaq HA. Int. J. Nanomed. 2013; 8:983–993.
23. Beckett WS, Chalupa DF, Pauly-Brown A, Speers DM, Stewart JC, Frampton MW, Utell MJ, Huang LS, Cox C, Zareba W, Oberdorster G. Am. J. Respir. Crit. Care Med. 2005; 171:1129–1135. [PubMed: 15735058]
24. Watson C, Ge J, Cohen J, Pyrgiotakis G, Engelward B, Demokritou P. 2013 **submitted**.
25. Sharma V, Shukla RK, Saxena N, Parmar D, Das M, Dhawan A. Toxicol. Lett. 2009; 185:211–218. [PubMed: 19382294]
26. Xia T, Zhao Y, Sager T, George S, Pokhrel S, Li N, Schoenfeld D, Meng H, Lin S, Wang X, Wang M, Ji Z, Zink JI, Madler L, Castranova V, Lin S, Nel AE. ACS Nano. 2011; 5:1223–1235. [PubMed: 21250651]
27. Teleki A, Heine MC, Krumeich F, Akhtar MK, Pratsinis SE. Langmuir. 2008; 24:12553–12558. [PubMed: 18850688]
28. Cabot Corp. "CAB-O-SIL® Fumed silica in cosmetic and personal care products" Report. 2001
29. Brunner TJ, Wick P, Manser P, Spohn P, Grass RN, Limbach LK, Bruinink A, Stark WJ. Environ. Sci. Technol. 2006; 40:4374–4381. [PubMed: 16903273]
30. Napierska D, Thomassen LCJ, Rabolli V, Lison D, Gonzalez L, Kirsch-Volders M, Martens JA, Hoet PH. Small. 2009; 5:846–853. [PubMed: 19288475]
31. Zhang H, Dunphy DR, Jiang X, Meng H, Sun B, Tarn D, Xue M, Wang X, Lin S, Ji Z, Li R, Garcia FL, Yang J, Kirk ML, Xia T, Zink JI, Nel A, Brinker CJ. J. Am. Chem. Soc. 2012; 134:15790–15804. [PubMed: 22924492]
32. Warheit DB, McHugh TA, Hartsky MA. Scand. J. Work Environ. Health. 1995; 21:19–21. [PubMed: 8929682]
33. Demokritou P, Gass S, Pyrgiotakis G, Cohen JM, Goldsmith W, McKinney W, Frazer D, Ma J, Schwegler-Berry D, Brain J, Castranova V. Nanotoxicology. 2013; 7:1338–1350. [PubMed: 23061914]
34. Sotiriou GA, Sannomiya T, Teleki A, Krumeich F, Voeroes J, Pratsinis SE. Adv. Funct. Mater. 2010; 20:4250–4257. [PubMed: 23730266]
35. Sotiriou GA, Franco D, Poulikakos D, Ferrari A. ACS Nano. 2012; 6:3888–3897. [PubMed: 22509739]
36. Demokritou P, Buechel R, Molina RM, Deloid GM, Brain JD, Pratsinis SE. Inhal. Toxicol. 2010; 22:107–116. [PubMed: 20701428]
37. Weingeist DM, Ge J, Wood DK, Mutamba JT, Huang Q, Rowland EA, Yaffe MB, Floyd S, Engelward BP. Cell Cycle. 2013; 12:907–915. [PubMed: 23422001]
38. Cohen J, DeLoid G, Pyrgiotakis G, Demokritou P. Nanotoxicology. 2013; 7:417–431. [PubMed: 22393878]
39. Darrah TH, Prutsman-Pfeiffer JJ, Poreda RJ, Campbell ME, Hauschka PV, Hannigan RE. Metallomics. 2009; 1:479–488. [PubMed: 21305156]
40. Sprauten M, Darrah TH, Peterson DR, Campbell ME, Hannigan RE, Cvancarova M, Beard C, Haugnes HS, Fossa SD, Oldenburg J, Travis LB. J. Clin. Oncol. 2012; 30:300–307. [PubMed: 22184390]
41. Kimura A, Miyata A, Honma M. Mutagenesis. 2013; 28:583–590. [PubMed: 23863314]
42. Walmsley, R.; Tate, M. The GADD45a-GFP GreenScreen HC Assay. In: Parry, JM.; Parry, EM., editors. Genetic Toxicology. Vol. Vol. 817. New York: Springer; 2012. p. 231-250.

43. Wood DK, Weingeist DM, Bhatia SN, Engelward BP. Proc. Natl. Acad. Sci. U. S. A. 2010; 107:10008–10013. [PubMed: 20534572]
44. Ulrich GD. Chem. Eng. News. 1984; 62:22–29. [PubMed: 11541976]
45. Hembram K, Sivaprakasam D, Rao TN, Wegner K. J. Nanopart. Res. 2013; 15:1461.
46. Height MJ, Madler L, Pratsinis SE, Krumeich F. Chem. Mater. 2006; 18:572–578.
47. Teleki A, Akhtar MK, Pratsinis SE. J. Mater. Chem. 2008; 18:3547–3555.
48. Tani T, Madler L, Pratsinis SE. Part. Part. Syst. Charact. 2002; 19:354–358.
49. Madler L, Kammler HK, Mueller R, Pratsinis SE. J. Aerosol Sci. 2002; 33:369–389.
50. Sotiriou GA, Schneider M, Pratsinis SE. J. Phys. Chem. C. 2012; 116:4493–4499.
51. Jung R, Lee JC, Orosz GT, Sulyok A, Zsolt G, Menyhard M. Surf. Sci. 2003; 543:153–161.
52. Teleki A, Buesser B, Heine MC, Krumeich F, Akhtar MK, Pratsinis SE. Ind. Eng. Chem. Res. 2008; 48:85–92.
53. Liufu S, Xiao H, Li YP. Powder Technol. 2004; 145:20–24.
54. Sotiriou GA, Hirt AM, Lozach P-Y, Teleki A, Krumeich F, Pratsinis SE. Chem. Mater. 2011; 23:1985–1992. [PubMed: 23729990]
55. Height MJ, Pratsinis SE, Mekasuwandumrong O, Praserthdam P. 2006; 63:305–312.
56. Pratsinis SE. AIChE J. 2010; 56:3028–3035.
57. Mueller R, Kammler HK, Wegner K, Pratsinis SE. Langmuir. 2003; 19:160–165.
58. Deligiannakis Y, Sotiriou GA, Pratsinis SE. ACS Appl. Mater. Interfaces. 2012; 4:6609–6617. [PubMed: 23121088]
59. Teleki A, Suter M, Kidambi PR, Ergeneman O, Krumeich F, Nelson BJ, Pratsinis SE. Chem. Mater. 2009; 21:2094–2100.
60. Han Y, Jiang J, Lee SS, Ying JY. Langmuir. 2008; 24:5842–5848. [PubMed: 18465888]
61. Zhang H, Ji Z, Xia T, Meng H, Low-Kam C, Liu R, Pokhrel S, Lin S, Wang X, Liao Y-P, Wang M, Li L, Rallo R, Damoiseaux R, Telesca D, Maedler L, Cohen Y, Zink JI, Nel AE. ACS Nano. 2012; 6:4349–4368. [PubMed: 22502734]
62. Cohen JM, Derk R, Rojanasakul L, Godleski J, Kobzik L, Brain J, Demokritou P. Nanotoxicology. 2014 **in press**.
63. Kiskinis E, Suter W, Hartmann A. Mutagenesis. 2002; 17:37–43. [PubMed: 11752232]
64. George S, Pokhrel S, Xia T, Gilbert B, Ji Z, Schowalter M, Rosenauer A, Damoiseaux R, Bradley KA, Maedler L, Nel AE. ACS Nano. 2010; 4:15–29. [PubMed: 20043640]

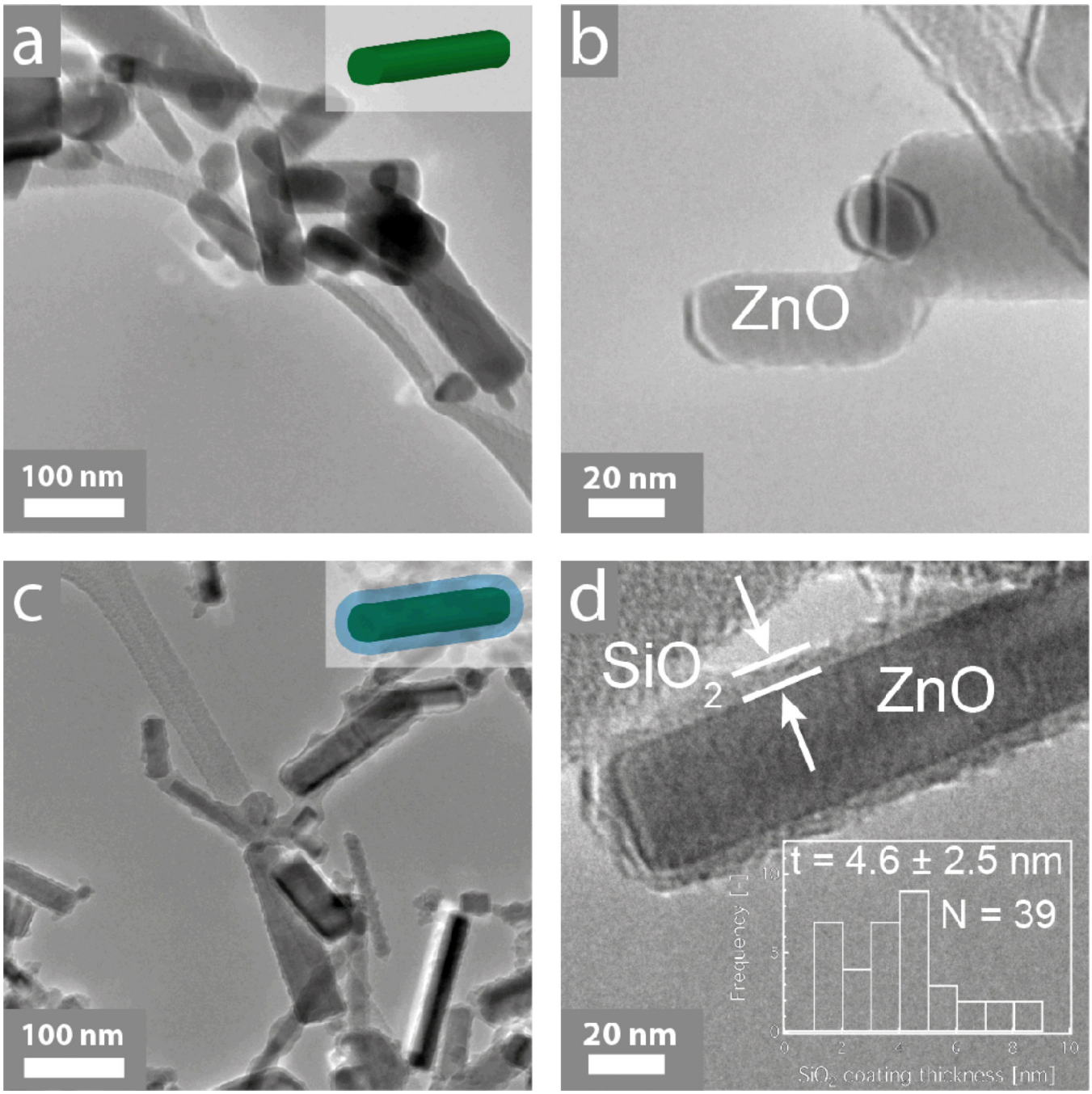

Figure 1.

Transmission electron microscopy images of the uncoated (a, b) and SiO_2-coated ZnO nanoparticles. In both cases, the ZnO forms nanorods with aspect ratio ~3:1. Furthermore, there is a nanothin amorphous SiO_2 shell encapsulating the core particles for the SiO_2-coated ZnO nanorods. In the inset of (d) the SiO_2 coating thickness distribution along with the average coating thickness ± standard deviation and the total number N of coatings counted.

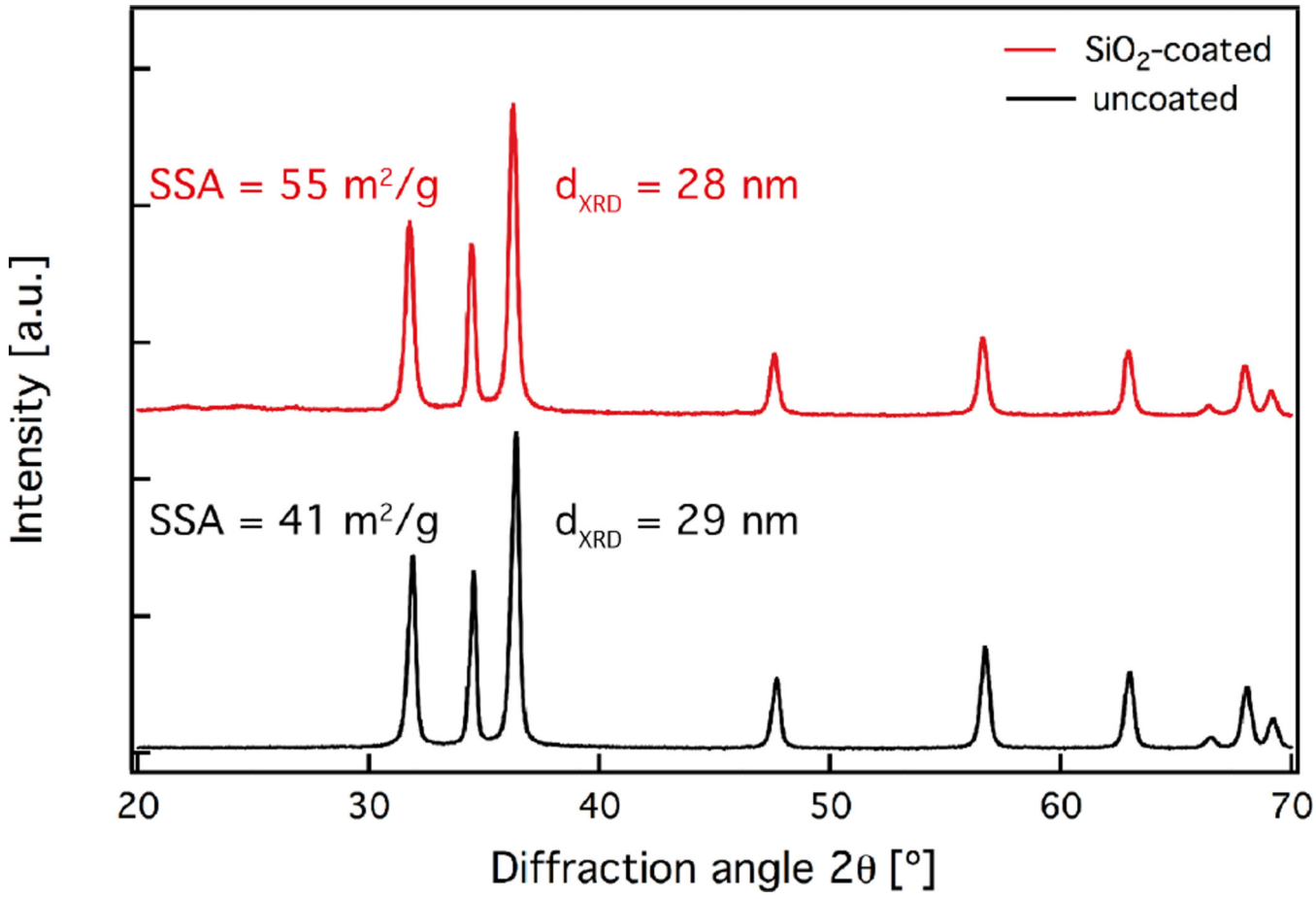

Figure 2.
X-ray diffraction patterns of the uncoated (black line) and SiO_2-coated ZnO nanorods (red line). Their average crystal size (d_{XRD}) and specific surface area (SSA) values are also displayed.

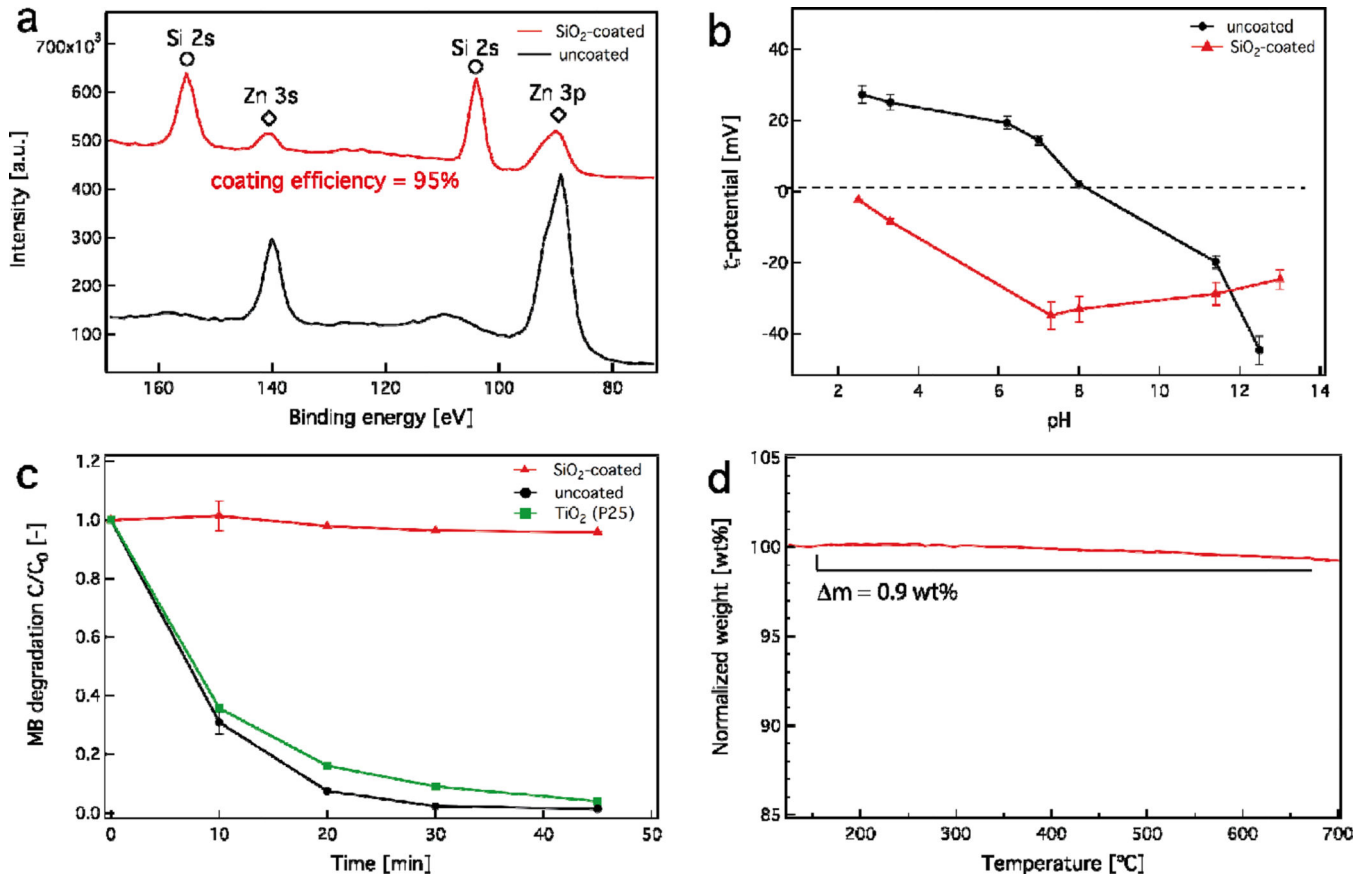

Figure 3.

(a) X-ray photoelectron spectroscopy of uncoated (black line) and SiO_2-coated ZnO nanorods (red line). The Zn (diamonds) and Si (circles) binding energy peaks are also shown. The SiO_2 coating efficiency is also displayed. (b) The ζ-potential of both uncoated (black line) and SiO_2-coated ZnO nanorods. (c) The methylene blue (MB) degradation over time of the uncoated (black line) and SiO_2-coated ZnO nanorods (red line) upon UV irradiation. The MB degradation of TiO_2 (green line, P25) is also shown as a positive control. (d) Thermogravimetric analysis of the SiO_2-coated ZnO nanorods. The mass loss is less than 1% indicating no organic species on the SiO_2 surface.

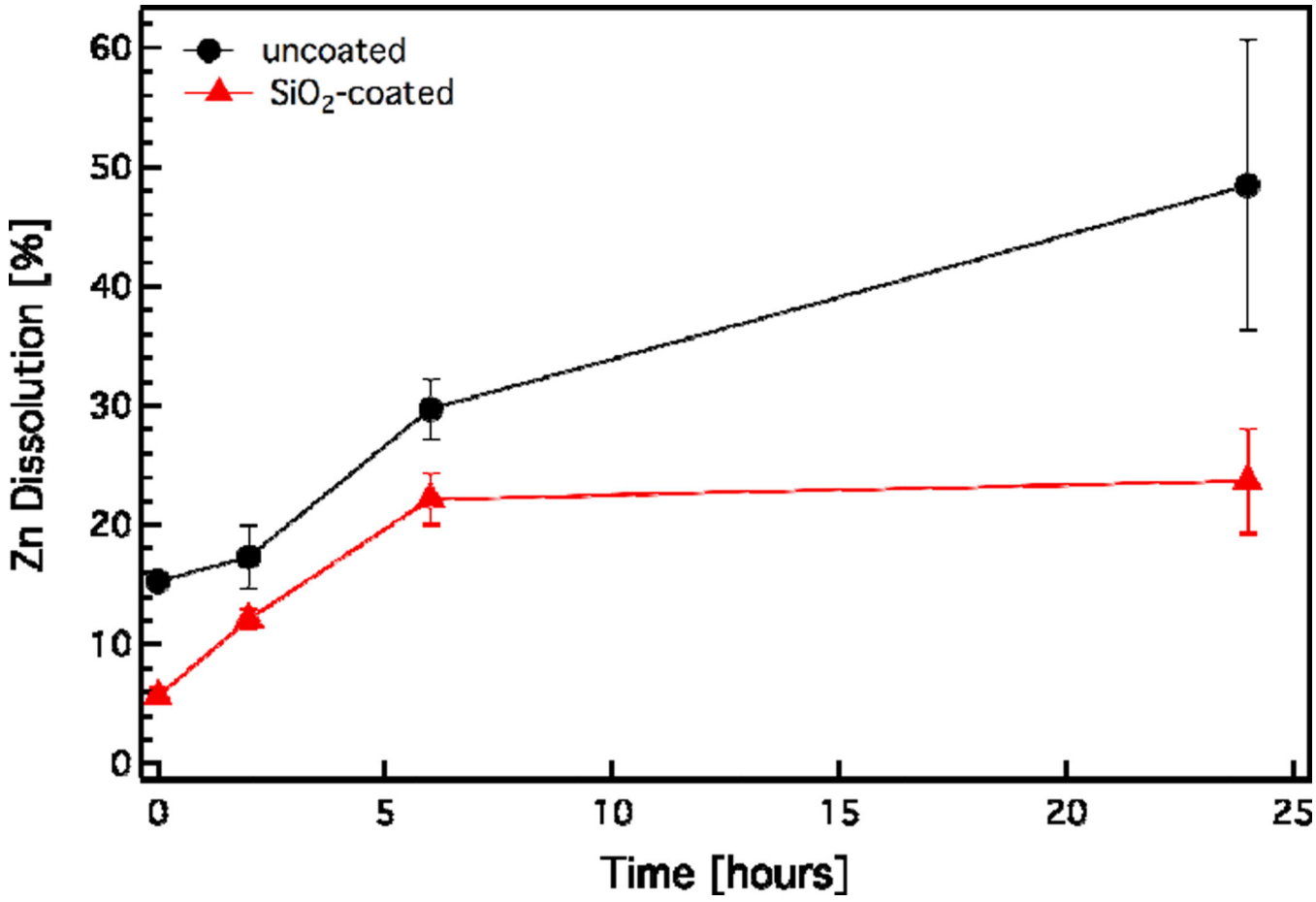

Figure 4.

The dissolution kinetics of uncoated (black circles) and SiO_2-coated ZnO nanorods (red triangles) in RPMI-1640 cell culture medium (pH = 7.4, total concentration of inorganic salts [ionic strength] = 139.1 mM) for initial ZnO concentration of 100 mg/L.

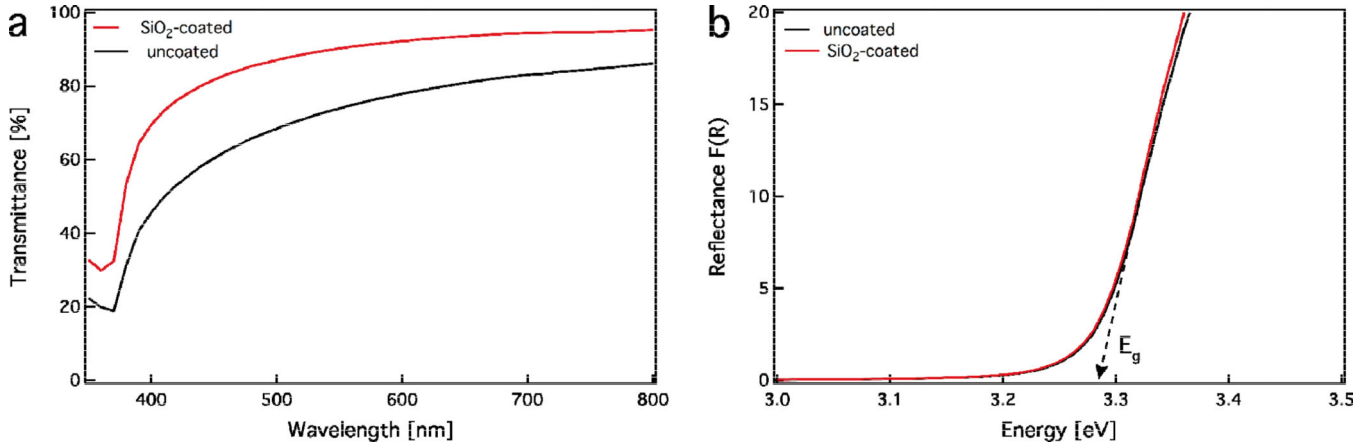

Figure 5.

(a) Optical transmission spectra of aqueous suspensions containing the uncoated (black line) and SiO_2-coated ZnO nanorods (red line) at concentration 0.5 mg/mL. The SiO_2-coated ZnO nanorods are more transparent in the visible spectrum because of their smaller agglomerate size. (b) Diffuse-reflectance measuremnts of dry powders of the uncoated (black line) and SiO_2-coated ZnO nanorods (red line). Both curves are identical and exhibit the same band-gap energy.

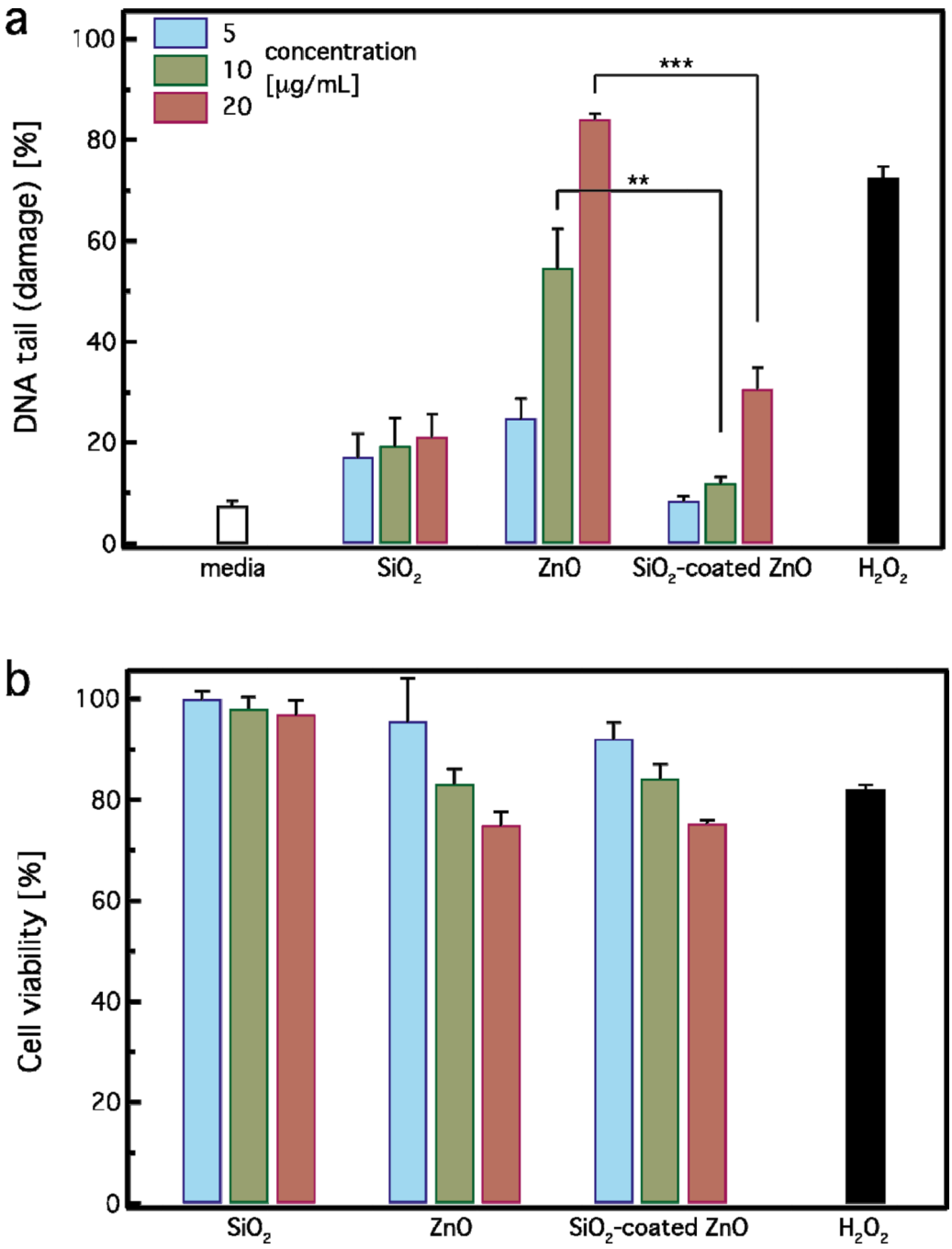

Figure 6.

(a) Single stranded DNA damage in TK6 cells after zinc oxide exposure using the Nano-Cometchip technology. Cells were treated with (5, 10, 20 µg/mL) of SiO_2-coated or uncoated ZnO nanorods for 4 hours. Positive control was 100 µM of hydrogen peroxide (H_2O_2) for 20 minutes. The results are expressed as mean + standard error of three independent experiments performed in triplicate. Thus, approximately 800 comets were analyzed for each treatment/dose. Values are significantly different in comparison to each

treatment SiO_2-coated vs. uncoated; **p-value < 0.01, ***p-value < 0.001. (b) Cell viability was determined by MTT assay after 4 hours.